OTFS Enabled RIS-Aided Localization: Fundamental Limits and Potential Drawbacks

Don-Roberts Emenonye, Anish Pradhan, Harpreet S. Dhillon, and R. Michael Buehrer

***Abstract*—In this paper, we consider a reconfigurable intelligent surface (RIS) aided orthogonal time frequency space (OTFS) system that can operate in either the near-field or far-field propagation regimes. The received signal expressions in the Doppler-delay (DD) are derived when the system experiences the effects of near-field or far-field propagation. Utilizing these received signal expressions and the Fisher information matrix (FIM), we derive the fundamental localization error limits of a user equipment (UE) that receives signals in the DD domain after reflections from the RISs. Through simulations, we show that the localization error decreases with the number of receive antennas and RIS elements. Subsequently, we note that RISs can become misoriented, i.e., their orientations can be disturbed after initial deployment. Hence, we investigate the possibility of exploiting the signals received at the UE in the DD domain to estimate the RIS orientation. Our simulation results indicate that the orientation of a certain RIS can only be estimated when the UE is experiencing the effects of near-field propagation with respect to that RIS. Through simulations, we show that a fundamental drawback of RIS-aided localization of a UE is that the RIS orientation offset is detrimental to the localization error of the UE.**

***Index Terms*—RIS, 6G localization, OTFS, RIS misorientation, near-field, Bayesian Fisher information.**

I. Introduction

Navigation systems for certain autonomous use cases must provide line-of-sight (LOS) and be able to deal with time-varying channels due to high Doppler. While the emerging idea of reconfigurable intelligent surfaces (RIS) in GPS-denied environments [1], [2] can provide a virtual LOS path by directing signals from a base station (BS) to a user equipment (UE) [3]–[6], the use of orthogonal time frequency space waveform (OTFS) can provide a means of handling the time-varying channels resulting from high Doppler [7]–[9].

Prior works on RIS-aided localization can be grouped into near-field [4]–[6], [10]–[13] and far-field propagation [3], [14]–[16]. The boundary between the near-field and far-field is specified by the the Fraunhofer distance [17]. In the near-field, the wavefront has substantial curvature with respect to the array it impinges upon. In the far-field, the waves have traveled a sufficient distance such that it appears to be a plane wave with respect to the array it impinges upon. In [3], the fundamental limits of RIS-aided wireless systems are presented, and the structure of these fundamental limits is investigated. The previous work extends from the far-field to the near-field in [5]. Also, the authors in [5] prove that under a particular class of reflection coefficients, the RIS orientation can only be estimated under the near-field propagation regime. In [6], the reflection coefficients of the RIS are optimized to reduce the fundamental error limits while the RIS is operating in the near-field. The work in [10] presents a vision of RIS-aided localization; this vision includes the impact of high operating center frequency and highly directive elements. The fundamental limits are derived starting from the received signals [11] and from Maxwell's equations in [12]. The work in [13] uses RISs as a lens receiver. In [14], the case of synchronization and localization is investigated with a single antenna UE. In [15], the RISs are non-stationary, and the fundamental limits are derived based on the signals obtained at a stationary UE. In [16], the RISs are stationary, and the fundamental limits are derived based on the signals obtained at a non-stationary UE.

To handle time-varying channels, a new waveform, termed OTFS, was introduced in [7]. In that work, the performance of communicating through this waveform is investigated under a single antenna BS and a single antenna UE framework. For this setup, a message passing detector is developed in [8]. The single input single output (SISO) is extended to a multiple input multiple output (MIMO) framework in [9]. However, there are just a couple of prior works focusing at the intersection of RISs and OTFS [18], [19]. In [18], the expressions of the received signals for an RIS-assisted OTFS communication system are presented for both the Doppler-delay (DD) and the time-frequency (TF) domains. Authors in that work also investigate a channel estimation scheme and present the system's bit error rate. Finally, authors in [19] show that RISs improve the performance of a communication system that uses the OTFS waveform.

While these initial works on RIS-aided OTFS systems have been encouraging, no works have investigated the possibility of using RIS-aided OTFS systems for localization. Also, no prior works have derived received signal expressions in the DD domain for a UE operating in the near-field propagation regime. Hence, in this work, we present expressions for signals received while the UE is

D.-R. Emenonye, A. Pradhan, H. S. Dhillon, and R. M. Buehrer are with Wireless@VT, Bradley Department of Electrical and Computer Engineering, Virginia Tech, Blacksburg, VA, 24061, USA. Email: {donroberts, pradhananish1, hdhillon, rbuehrer}@vt.edu. The support of the US National Science Foundation (Grants ECCS-2030215 and CNS-2107276) is gratefully acknowledged.

experiencing the effects of near-field propagation in the DD domain. Subsequently, through the Fisher information matrix (FIM), we derive the fundamental localization error limits of a UE that receives signals in the DD domain after reflections from RISs.

It is also important to note that due to the possibility of ubiquitous deployment of RISs, the RISs can become misoriented after deployment. More specifically, the orientation of the RISs can be disturbed after deployment. Hence, in this work, we also investigate the possibility of using the signals received at the UE in the DD domain to estimate the RIS orientation. For completeness, the study of misorientation is performed in both the near-field and far-field propagation regimes.

Notation: The superscript $(\cdot)^{[0]}$ is related to the LOS path; the superscript $(\cdot)^{[m]}, m \in \{1, 2, \cdots, M_1\}$, is related to the m^{th} RIS path; subscripts which are upper case letters represents the centroid of the appropriate communication entity, i.e., (BS, RISs, and UE); subscripts which are lower case letters represents the numbering of the element on the appropriate communication entity; the transpose operator is $(\cdot)^{\mathrm{T}}$; the hermitian transpose operator is $(\cdot)^{\mathrm{H}}$; the complex conjugate operator is $(\cdot)^*$; the operation $[\boldsymbol{V}]_{[g_1:v_1, g_2:v_2]}$ extracts the submatrix represented by both the rows that lie in the range, $g_1{:}v_1$, and the columns that lie in the range $g_2{:}v_2$ of the matrix $\boldsymbol{V}$; the operator for the Euclidean norm is $\|\cdot\|$.

II. System Model

We consider an RIS-assisted OTFS system with N_B antennas at a single BS and N_U antennas at a single UE. There are $N_R^{[m]}$ reflecting elements on the m^{th} RIS where $m \in \mathcal{M}_1 = \{1, 2, \cdots, M_1\}$. The BS, RISs, and UE have arbitrary but known array geometry. The general system model is illustrated in Fig. 1. Note that the LoS part of the received signal is assumed blocked when we present the numerical results. In this paper, the BS, RISs, and UE are referred to as communication entities.

The centroid of BS is located at $\boldsymbol{p}_B = [x_B, y_B, z_B]^{\mathrm{T}} \in \mathbb{R}^3$, and the b^{th} antenna on this entity is located at $\boldsymbol{s}_b \in \mathbb{R}^3$, where the point $\boldsymbol{s}_b$ is defined with respect to the centroid of the BS. This point, $\boldsymbol{s}_b$, is also defined with respect to the global reference point as $\boldsymbol{p}_b = \boldsymbol{p}_B + \boldsymbol{s}_b$. The point, $\boldsymbol{s}_b$, can also be written as $\boldsymbol{s}_b = \boldsymbol{Q}_B \tilde{\boldsymbol{s}}_b$, where $\boldsymbol{Q}_B = \boldsymbol{Q}_B(\alpha_B, \psi_B, \varphi_B)$ is a 3D rotation matrix [20], and $\tilde{\boldsymbol{s}}_b$ is the equivalent point when the position of the b^{th} antenna on the BS is defined with respect to the global reference axis. The centroid (located at $\boldsymbol{p}_Q$) of an entity with collection of elements, $q \in \{1, 2, \cdots, N_Q\}$, can be described with respect to the centroid of another entity (located at $\boldsymbol{p}_E$) with collection of elements, $e \in \{1, 2, \cdots, N_E\}$, as $\boldsymbol{p}_Q = \boldsymbol{p}_E + d_{E,Q}\boldsymbol{\Delta}_{E,Q}$, where $d_{E,Q}$ is the distance from point $\boldsymbol{p}_E$ to point $\boldsymbol{p}_Q$ and $\boldsymbol{\Delta}_{E,Q}$ is the corresponding unit direction vector $\boldsymbol{\Delta}_{E,Q} = [\cos\phi_{E,Q}\sin\theta_{E,Q}, \sin\phi_{E,Q}\sin\theta_{E,Q}, \cos\theta_{E,Q}]^{\mathrm{T}}$. The point corresponding to the e^{th} element on the entity with centroid located at $\boldsymbol{p}_E$ is defined as $\boldsymbol{w}_e = d_{\boldsymbol{w}_e}\boldsymbol{\Delta}_{\boldsymbol{w}_e}$, where $\boldsymbol{w} \in \{\boldsymbol{s}, \tilde{\boldsymbol{s}}\}$, $d_{\boldsymbol{w}_e}$ is the distance from the centroid of the e^{th} entity to its e^{th} element, and $\boldsymbol{\Delta}_{\boldsymbol{w}_e}$ is the corresponding unit direction vector, $\boldsymbol{\Delta}_{\boldsymbol{w}_e} = [\cos\phi_{\boldsymbol{w}_e}\sin\theta_{\boldsymbol{w}_e}, \sin\phi_{\boldsymbol{w}_e}\sin\theta_{\boldsymbol{w}_e}, \cos\theta_{\boldsymbol{w}_e}]^{\mathrm{T}}$. The orientation angles of an entity located at $\boldsymbol{p}_E$ are vectorized as $\boldsymbol{\Phi}_E = [\alpha_E, \psi_E, \varphi_E]^{\mathrm{T}}$. *The delay from the e^{th} element on the entity with its centroid located at $\boldsymbol{p}_E$ to the q^{th} element on the entity with its centroid located at $\boldsymbol{p}_Q$ can be expressed as $\tau_{e,q} = d_{e,q}/c$, where $d_{e,q}$ and c are the distance and the speed of light, respectively. In the near-field, there is substantial curvature in the waves at the receiving end and the distance, $d_{e,q}$ is specified by the Euclidean norm. More specifically, $d_{e,q} = \|\boldsymbol{p}_q - \boldsymbol{p}_e\|$. In the far-field, the waves at the receiving end are plane, and the distance, $d_{e,q}$, can be specified by a first order Taylor series approximation of the Euclidean norm. More specifically, $d_{e,q} \approx d_{E,Q} + \Delta_{E,Q}^{\mathrm{T}}(\boldsymbol{s}_q - \boldsymbol{s}_e)$.*

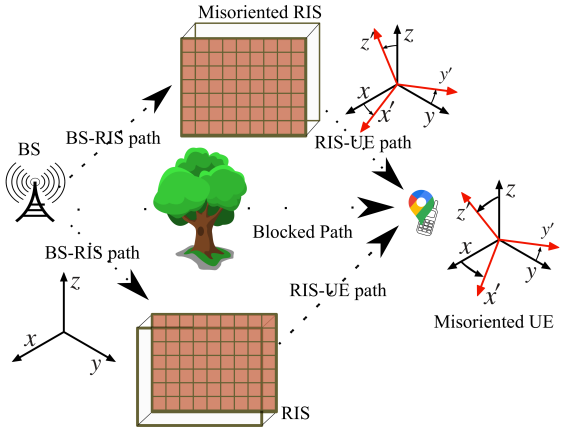

Figure 1. An illustration of the system model. While expressions for the LOS part of the received signal is presented, it is assumed blocked in the numerical results section.

In this work, we consider that the orientation angles of the m^{th} RIS, $\boldsymbol{\Phi}^{[m]}$, are initially known to the UE. However, over time the RISs can become misoriented, and the information on the orientation of certain RISs can become outdated. In this situation, the orientation offsets become parameters that must be estimated at the UE. Hence, in this paper, we characterize the fundamental error bound on the positioning accuracy of a UE under the presence and absence of RIS orientation offsets. We also characterize the fundamental error bound on the RISs' orientation offset estimation error. To enable these characterizations under OTFS transmissions, we derive signal representations about received signals transmitted by a BS, possibly reflected by an RIS, and received by a UE in the DD domain. With these signal representations, we use the FIM to quantify the available information for UE positioning, and RIS orientation offset estimation.

A. Transmit Processing

The OTFS frame is T seconds in the delay domain and $\Delta f = 1/T$ in the Doppler domain, and this frame is sub-divided into $N_n N_w$ DD resource elements by creating $\Delta f/N_n$ divisions in the Doppler domain and T/N_w divisions in the delay domain. A single Doppler delay resource element (DDRE) contains at most one communication symbol, and is indexed with $k = 0, 1, \ldots, N_n$ along the Doppler domain and $p = 0, 1, \ldots, N_w$ along the delay domain. At the b^{th} antenna on the BS, a $N_n \times N_w$ frame, $\{\mathsf{x}_b[k,p]\}_{k=0,p=0}^{N_n-1,N_w-1}$, is created in the DD domain, and converts this frame from the DD domain to the TF domain using the Inverse Symplectic Finite Fourier Transform (ISFFT),

$$x_b[n,w] = \frac{1}{\sqrt{N_n N_w}} \sum_{k=0}^{N_n-1} \sum_{p=0}^{N_w-1} \mathsf{x}_b[k,p] e^{j2\pi\left(\frac{nk}{N_n} - \frac{wp}{N_w}\right)},$$
$$n = 0, 1, \ldots, N_n - 1, w = 0, 1, \ldots, N_w - 1.$$

Subsequently, the BS adds a CP of length N_{cp} and transforms the signal from the TF domain to the continuous time domain through a Heisenberg transform

$$A_{g_{\text{rx}},g_{\text{tx}}}(t,f) \triangleq \int g_{\text{rx}}^{*}(t'-t)\, g_{\text{tx}}(t')\, e^{-j2\pi f(t'-t)} dt',$$

where g_{tx} is the transmit pulse, and g_{rx} is the receive pulse.

B. Channel Model and Continuous TF Received Signal Representation

Definition 1. *Given the transmit and receive pulses specified by g_{tx} and g_{rx}, respectively, the cross-ambiguity function between the two pulses are*

$$x_b(t) = \sum_{n=-N_{cp}}^{N_n-1} \sum_{w=0}^{N_w-1} x_b[[n]_{N_n}, w] g_{tx}(t-nT) e^{j2\pi w\Delta f(t-nT)}.$$

The LOS channel between the b^{th} antenna on the BS and the u^{th} antenna on the UE is

$$\mathsf{h}_{b,u}(\tau,\nu) = \sum_{l=1}^{N_L} \beta_{l,b,u} \delta(\tau - \tau_{l,b,u}^{[0]}) \delta(\nu - \nu_{l,b,u}^{[0]}), \quad (1)$$

where $\tau_{l,b,u}^{[0]}$ and $\nu_{l,b,u}^{[0]}$ are the delay and Doppler associated with the l^{th} path between the b^{th} antenna on the BS and the u^{th} antenna on the UE. The corresponding complex path gains and the number of paths are specified by $\beta_{l,b,u}^{[0]}$ andN_L, respectively. The noise-free part of received signal along this path is

$$\mu_{b,u}^{[0]}(t) = \sum_{l=1}^{N_L} \beta_{l,b,u}^{[0]} s(t - \tau_{l,b,u}^{[0]}) e^{j2\pi\nu_{l,b,u}^{[0]}(t-\tau_{l,b,u}^{[0]})}. \quad (2)$$

This signal in the TF continuous domain, $\mu_{b,u}^{[0]}(t,f)$, after matched filtering is $\mu_{b,u}^{[0]}(t,f) = A_{g_{rx},\mu_{b,u}^{[0]}}(t,f)$. The channel associated with the RIS path between the b^{th} antenna on the BS and the r^{th} element on the m^{th} RIS is

$$\mathsf{h}_{b,r}^{[m]}(\tau,\nu) = \sum_{l_1=1}^{N_{L_1}} \beta_{l_1,b,r}^{[m]} \delta(\tau - \tau_{l_1,b,r}^{[m]}) \delta(\nu - \nu_{l_1,b,r}^{[m]}), \quad (3)$$

where $\tau_{l_1,b,r}^{[m]}$ and $\nu_{l_1,b,r}^{[m]}$ are the delay and Doppler associated with the l_1^{th} path between the b^{th} antenna on the e^{th} BS and the r^{th} element on the m^{th} RIS. The corresponding complex path gains and the number of paths are specified by $\beta_{l_1,b,r}^{[m]}$ andN_{L_1}, respectively. The noise-free part of received signal along this path is

$$\mu_{b,r}^{[m]}(t) = e^{j\vartheta_r^{[m]}} \sum_{l=1}^{N_{L_1}} \beta_{l_1,b,r}^{[m]} s(t - \tau_{l_1,b,r}^{[m]}) e^{j2\pi\nu_{l_1,b,r}^{[m]}(t-\tau_{l_1,b,r}^{[m]})}, \quad (4)$$

where $\vartheta_r^{[m]}$ is the phase of the r^{th} element of the m^{th} RIS. The channel associated with the RIS path between the r^{th} element on the m^{th} RIS and the u^{th} antenna on the UE is

$$\mathsf{h}_{r,u}^{[m]}(\tau,\nu) = \sum_{l_2=1}^{N_{L_2}} \beta_{l_2,r,u}^{[m]} \delta(\tau - \tau_{l_2,r,u}^{[m]}) \delta(\nu - \nu_{l_2,r,u}^{[m]}), \quad (5)$$

where $\tau_{l_2,r,u}^{[m]}$ and $\nu_{l_2,r,u}^{[m]}$ are the delay and Doppler associated with the l_2^{th} path between the r^{th} element on the m^{th} RIS and the u^{th} antenna on the UE. The corresponding complex path gains and the number of paths are specified by $\beta_{l_2,u,q}^{[m]}$ andN_{L_2}, respectively. The noise-free part of received signal along this path is

$$\mu_{r,u}^{[m]}(t) = \sum_{l=1}^{N_{L_2}} \beta_{l_2,r,u}^{[m]} \mu_{b,r}^{[m]}(t - \tau_{l_2,r,u}^{[m]}) e^{j2\pi\nu_{l_2,r,u}^{[m]}(t-\tau_{l_2,r,u}^{[m]})}. \quad (6)$$

This signal in the TF continuous domain, $\mu_{r,u}^{[m]}(t,f)$, after matched filtering is $\mu_{r,u}^{[m]}(t,f) = A_{g_{rx},\mu_{r,u}^{[m]}}(t,f)$.

C. Received Signal

Expressions for the received signal at the u^{th} antenna on the UE are obtained and presented in the following Lemmas and Corollaries.

Lemma 1. *After sampling at $t = nT$ and $f = w\Delta f$, the useful part of the signal in the TF domain that is received at the u^{th} antenna on the UE is*

$$\mu_u^{(1)}[n,w] = \sum_b \sum_{n'} \sum_{w'} x_b[n', w'] H_{b,u}[n', w'], \quad (7)$$

where the LOS channel is $H_{b,u}[n', w'] = \sum_{l=1}^{N_L} \beta_{l,b,u}^{[0]} A_{g_{rx},g_{tx}}((n-n')T - \tau_{l,b,u}^{[0]}), (w-w')\Delta f - \nu_{l,b,u}^{[0]}) e^{j2\pi w'\Delta f((n-n')T - \tau_{l,b,u}^{[0]})} e^{j2\pi\nu_{l,b,u}^{[0]}(nT-\tau_{l,b,u}^{[0]})}$. The useful part of the signal in the TF domain that is reflected

by the RISs and received at the u^{th} antenna on the UE is

$$\mu_u^{(2)}[n,w] = \sum_{m=1}^{M_1} \psi^{[m]} \times \Bigg[\sum_{r=1}^{N_R^{[m]}} e^{j\vartheta_r^{[m]}} \Bigg[\sum_b \sum_{n'} \sum_{w'} x_b[n',w'] H_{b,u}^{r,[m]}[n',w'] \Bigg] \Bigg], \tag{8}$$

where $\psi^{[m]}$ indicates the presence of an RIS-aided path from the BS to the UE, $H_{b,u}^{r,[m]}[n',w'] = \sum_{l_1=1}^{N_{L_1}} \sum_{l_2=1}^{N_{L_2}} \beta_{l_1,b,r}^{[m]} \beta_{l_2,r,u}^{[m]} A_{g_{rx},g_{tx}}((n-n')T - (\tau_{l_1,b,r}^{[m]} + \tau_{l_2,r,u}^{[m]}), (w-w')\Delta f - (\nu_{l_1,b,r}^{[m]} + \nu_{l_2,r,u}^{[m]})) e^{j2\pi w' \Delta f((n-n')T - (\tau_{l_1,b,r}^{[m]} + \tau_{l_2,r,u}^{[m]}))} \times e^{j2\pi(\nu_{l_1,b,r}^{[m]} + \nu_{l_2,r,u}^{[m]})(nT - (\tau_{l_1,b,r}^{[m]} + \tau_{l_2,r,u}^{[m]}))} e^{j2\pi\nu_{l_2,r,u}^{[m]} \tau_{l_1,b,r}^{[m]}}$.

Proof. The expressions are obtained after sampling at $t = nT$ and $f = w\Delta f$ and appropriate manipulations. Detailed proof can be obtained by following the technique presented in [8]. Because of the near-field considerations, each BS antenna and UE antenna path can be viewed as a SISO path. Hence, the expressions for the LOS part of the signal can be obtained by following the technique presented in [8] while considering each BS antenna and UE antenna path similar to the SISO path in [8].

For the RIS part of the expressions, the proof is similar to the proof presented for SISO links in [8]. The difference is that there are two composite SISO paths in every BS antenna to RIS element to UE antenna, path. The first is from the BS antenna to the RIS element, and the second is from the RIS element to the UE antenna. Hence, the derivations are two-part. In the first part, the signal's expression at a specific element of an RIS can be viewed similarly to the expression at the receiver in [8]. In the second part, the signal at a specific element of an RIS is similar to the transmit signal in [8], and the signal at the receiver after reflections from the RIS is obtained by performing appropriate manipulations on this transmit signal. □

Corollary 1. *The useful part of the signal in the TF domain from both the LOS path and the RISs, which is received at the u^{th} antenna on the UE, is*

$$\mu_u[n,w] = \mu_u^{(1)}[n,w] + \mu_u^{(2)}[n,w]. \tag{9}$$

Proof. The proof is straightforward, as the useful part of the signal is the sum of the LOS signal and the signals reflected by the RISs. □

Definition 2. *Considering the LOS path and all the RIS paths, the delay τ_{max} and Doppler ν_{max} are the maximum delay and maximum Doppler, respectively.*

D. OTFS with Rectangular Waveforms

Ideal waveforms are impractical because they posit that a DD element is localizable in time and frequency without ambiguity in either domain. A practical waveform is a rectangular waveform that constrains a DD element to a specific range in the time domain with the caveat that this element is unconstrained in frequency.

Assumption 1. *The rectangular pulses have an amplitude $1/\sqrt{T}$ and exist in the time interval $t \in [0,T]$. The duration of the rectangular pulses have the property, $T \gg \tau_{\max}$.*

With rectangular transmit, rectangular receive waveforms, and Assumption 1, the cross ambiguity function in the TF, $A_{g_{\rm rx},g_{\rm tx}}((n-n')T - \tau, (w-w')\Delta f - \nu)$ is non-zero for $|\tau| < \tau_{\max}, |\nu| < \nu_{\max}$ only when $n' = n$ and $n' = n-1$. This section presents representations of the received signal when both the BS and UE employ rectangular pulses.

Lemma 2. *With rectangular transmit and receive waveforms, the useful part of the LOS signal in the TF domain that is received at the u^{th} antenna on the UE is*

$$\begin{aligned} \mu_u^{(1)}[n,w] &= \sum_b \sum_{n'=n-1}^{n} \sum_{w'} x_b[n',w'] H_{b,u}[n',w'] \\ &= \sum_b \Bigg[x_b[n,w] H_{b,u}[n,w] \\ &\quad + \sum_{w',w' \neq w} x_b[n,w'] H_{b,u}[n,w'] \\ &\quad + \sum_{w'} x_b[n-1,w'] H_{b,u}[n-1,w'] \Bigg]. \end{aligned} \tag{10}$$

The channel $H_{b,u}[n',w']$ is obtained from (7) by appropriate substitutions. The first term in the second equation describes the signals from the BS received at the w^{th} frequency subcarrier during the n^{th} time interval. The second term represents the interference from the other $N_w - 1$ subcarriers during the n^{th} time interval, and it is viewed as intercarrier interference at the u^{th} antenna on the UE received from the BS. The third term in the second equation represents the intersymbol interference due to the signals transmitted during previous time interval by the BS.

Proof. Because of the near-field considerations, each BS antenna and UE antenna path can be viewed as a SISO path. Hence, the expressions can be obtained by following the technique presented in [8] while considering each BS antenna and UE antenna path similar to the SISO path in [8]. □

Corollary 2. *Note that the received signal in (10) can be written as*

$$\mu_u^{(1)}[n,w] = \mu_u^{(1,1)}[n,w] + \mu_u^{(1,2)}[n,w], \tag{11}$$

where $\mu_u^{(1,1)}[n,w]$ is the sum of signal of interest and the intercarrier interference and $\mu_u^{(1,2)}[n,w]$ is the intersymbol interference.

Lemma 3. *The useful part of the signal in the TF domain that is reflected by the RISs and received at the u^{th} antenna on the UE is*

$$\mu_u^{(2)}[n,w] = \sum_{m=1}^{M_1} \psi^{[m]} \times \Bigg[\sum_{r=1}^{N_R^{[m]}} e^{j\vartheta_r^{[m]}} \Bigg[\sum_b \sum_{n'=n-1}^{n} \sum_{w'} x_b[n',w'] H_{b,u}^{r,[m]}[n',w'] \Bigg] \Bigg], \tag{12}$$

where the channel $H_{b,u}^{r,[m]}[n',w']$ is obtained from (8) by appropriate substitutions. Similar to (10), the equation in (12) can be decomposed into signal of interest, intercarrier interference, and intersymbol interference.

Proof. The derivations are two-part. In the first part, the signal's expression at a specific element of an RIS can be viewed similarly to the expression at the receiver in [8]. In the second part, the signal at a specific element of an RIS is similar to the transmit signal in [8], and the signal at the receiver after reflections from the RIS is obtained by performing appropriate manipulations on this transmit signal. □

Corollary 3. *The received signal in (12) can be written as*

$$\mu_u^{(2)}[n,w] = \mu_u^{(2,1)}[n,w] + \mu_u^{(2,2)}[n,w], \tag{13}$$

where $\mu_u^{(2,1)}[n,w]$ is the sum of signal of interest and the intercarrier interference and $\mu_u^{(2,2)}[n,w]$ is the intersymbol interference.

After the SFFT application to the signals in the TF domain represented by (10) and (11), the signals in the DD domain at the u^{th} antenna on the UE received through the LOS paths are presented as

$$\mu_u^{(1)}[k,p] = \mu_u^{(1,1)}[k,p] + \mu_u^{(1,2)}[k,p], \tag{14}$$

Lemma 4. *The entries in (14) are described as*

$$\mu_u^{(1,a)}[k,p] = \frac{1}{N_n N_w^2} \Bigg[\sum_b \sum_{k'} \sum_{p'} \mathsf{x}_b[k',p'] H_{b,u}[k',p'] \Bigg], \tag{15}$$

where $a \in \{1,2\}$, and the channel is given by (22). If $a = 1$ then $p' \in [0, N_w - 1 - p_{l,b,u}]$, $a = 2$ then $p' \in [N_w - p_{l,b,u}, N_w - 1]$. Now, $p_{l,b,u} = \tau_{l,b,u} N_w \Delta f$.

Proof. The proof follows the proof presented for SISO links in [8] while considering each BS antenna and UE antenna path as a distinct SISO link. □

After the SFFT application to the signals in the TF domain which are received at the u^{th} antenna on the UE through reflections from the RISs; the TF doamins signals represented by (12) and (13) are transformed to the DD domain and represented by

$$\mu_u^{(2)}[k,p] = \mu_u^{(2,1)}[k,p] + \mu_u^{(2,2)}[k,p], \tag{16}$$

Lemma 5. *The entries in (16) are described as*

$$\mu_u^{(2,a)}[k,p] = \frac{1}{N_w^2 N_n} \times \sum_{m=1}^{M_1} \psi^{[m]} \sum_b \sum_{r=1}^{N_R^{[m]}} e^{j\vartheta_r^{[m]}} \sum_{k'} \sum_{p'} \mathsf{x}_b[k',p'] \Big[H_{b,u}^{r,[m]}[k',p'] \Big], \tag{17}$$

where $a \in \{1,2\}$, and the channel is (23). If $a = 1$ then $p' \in [0, N_w - (p_{l_1,b,r}^{[m]} + p_{l_2,r,u}^{[m]}) - 1]$, $a = 2$ then $p' \in [N_w - (p_{l_1,b,r}^{[m]} + p_{l_2,r,u}^{[m]}), N_w - 1]$. We also define, $p_{l_1,b,r}^{[m]} = \tau_{l_1,b,r}^{[m]} N_w \Delta f$ and $p_{l_2,r,u}^{[m]} = \tau_{l_2,r,u}^{[m]} N_w \Delta f$ as delay taps.

Proof. The proof is similar to the proof presented for SISO links in [8]. The difference is that there are two composite SISO paths in every BS antenna to RIS element to UE antenna path. The first is from the BS antenna to the RIS element, and the second is from the RIS element to the UE antenna. □

Corollary 4. *The useful part of the signal in the DD domain from both the LOS path and the RISs, which is received at the u^{th} antenna on the UE, is*

$$\mu_u[k,p] = \mu_u^{(1)}[k,p] + \mu_u^{(2)}[k,p]. \tag{18}$$

Proof. The proof is straightforward, as the useful part of the signal is the sum of the LOS signal and the signals reflected by the RISs. □

Assumption 2. *The only scatters/reflectors are the RISs. Consequentially, $N_L = 1$, $N_{L_1} = 1$, and $N_{L_2} = 1$. Hence, the subscripts l, l_1, and l_2 are dropped from all equations after this point.*

III. Available Information in the Received Signal

The available information about channel parameters present in the received signal determines the performance of localization and communication systems. In this section, we specify these channel parameters by dividing the channel parameters into useful parameters and nuisance parameters.

A. Parameters in the Received Signal

The channel parameters in the LOS path are vectorized and have the following representation $\boldsymbol{\eta}^{[0]} \triangleq \left[\tau_{B,U}^{[0]}, \nu_{B,U}^{[0]}, \theta_{B,U}^{[0]}, \phi_{B,U}^{[0]}, \boldsymbol{\Phi}_U, \beta_{\text{R}}^{[0]}, \beta_{\text{I}}^{[0]}\right]^{\text{T}} = \left[\boldsymbol{\eta}_1^{[0]\text{T}}, \boldsymbol{\eta}_2^{[0]\text{T}}\right]^{\text{T}}$, such that the LOS related useful parameters is $\boldsymbol{\eta}_1^{[0]} = \left[\tau_{B,U}^{[0]}, \nu_{B,U}^{[0]}, \theta_{B,U}^{[0]}, \phi_{B,U}^{[0]}, \boldsymbol{\Phi}_U\right]^{\text{T}}$ represents and $\boldsymbol{\eta}_2^{[0]} = [\beta_{\text{R}}^{[0]}, \beta_{\text{I}}^{[0]}]^{\text{T}}$ represents the LOS related nuisance parameters. The variables $\beta_{\text{R}}^{[0]}$, $\beta_{\text{I}}^{[0]}$ represents the real and imarginary part of $\beta_{\text{B,U}}^{[0]}$, respectively. The orientation of the UE is placed in the LOS parameter vector for notational simplicity. The channel parameters in the m^{th}

RIS-aided path have the following representation $\boldsymbol{\eta}^{[m]} \triangleq \left[\tau_{R,U}^{[m]}, \nu_{R,U}^{[m]}, \theta_{R,U}^{[m]}, \phi_{R,U}^{[m]}, \boldsymbol{\Phi}_R^{[m]}, \beta_{\mathrm{R}}^{[m]}, \beta_{\mathrm{I}}^{[m]}\right]^{\mathrm{T}}$ $= \left[\boldsymbol{\eta}_1^{[m]\mathrm{T}}, \boldsymbol{\eta}_2^{[m]\mathrm{T}}\right]^{\mathrm{T}}$, such that $\boldsymbol{\eta}_1^{[m]} = \left[\tau_{R,U}^{[m]}, \nu_{R,U}^{[m]}, \theta_{R,U}^{[m]}, \phi_{R,U}^{[m]}, \boldsymbol{\Phi}_R^{[m]}\right]^{\mathrm{T}}$ represents the m^{th} RIS-aided related useful parameters and $\boldsymbol{\eta}_2^{[m]} = [\beta_{\mathrm{R}}^{[m]}, \beta_{\mathrm{I}}^{[m]}]^{\mathrm{T}}$ represents the m^{th} RIS-aided related nuisance parameters. The variables $\beta_{\mathrm{R}}^{[m]}$, $\beta_{\mathrm{I}}^{[m]}$ represents the real and imarginary part of $\beta_{\mathrm{B,R}}^{[m]} \times \beta_{\mathrm{R,U}}^{[m]}$, respectively.

All parameters can be collected as $\boldsymbol{\eta} \triangleq \left[\boldsymbol{\eta}^{[0]\mathrm{T}}, \boldsymbol{\eta}^{[1]\mathrm{T}}, \boldsymbol{\eta}^{[2]\mathrm{T}}, \cdots, \boldsymbol{\eta}^{[M_1]\mathrm{T}}\right]^{\mathrm{T}}$, where the channel parameters can also be divided into useful channel parameters, $\boldsymbol{\eta}_1^{[m]}$, and the nuisance parameters, $\boldsymbol{\eta}_2^{[m]}$, such that $\boldsymbol{\eta}^{[m]} \triangleq \left[\boldsymbol{\eta}_1^{[m]\mathrm{T}}, \boldsymbol{\eta}_2^{[m]\mathrm{T}}\right]^{\mathrm{T}}$.

B. Fisher Information Matrix

One way of quantifying the information about channel parameters (deterministic or random) present in random observations of the received signal is through the FIM. Mathematically, the general FIM of a parameter vector $\boldsymbol{\eta}$ is defined as

$$\begin{aligned}\mathbf{J}_{\boldsymbol{y};\boldsymbol{\eta}} &\triangleq \mathbb{E}_{\boldsymbol{y};\boldsymbol{\eta}}\left[-\frac{\partial^2 \ln \chi(\boldsymbol{y};\boldsymbol{\eta})}{\partial\boldsymbol{\eta}\partial\boldsymbol{\eta}^{\mathrm{T}}}\right] \\ &= -\mathbb{E}_{\boldsymbol{y}}\left[\frac{\partial^2 \ln \chi(\boldsymbol{y}|\boldsymbol{\eta})}{\partial\boldsymbol{\eta}\partial\boldsymbol{\eta}^{\mathrm{T}}}\right] - \mathbb{E}_{\boldsymbol{\eta}}\left[\frac{\partial^2 \ln \chi(\boldsymbol{\eta})}{\partial\boldsymbol{\eta}\partial\boldsymbol{\eta}^{\mathrm{T}}}\right] \\ &= \mathbf{J}_{\boldsymbol{y}|\boldsymbol{\eta}} + \mathbf{J}_{\boldsymbol{\eta}},\end{aligned} \tag{19}$$

where $\chi(\boldsymbol{y};\boldsymbol{\eta})$ denotes the probability density function (PDF) of $\boldsymbol{y}$ and $\boldsymbol{\eta}$, $\chi(\boldsymbol{y}|\boldsymbol{\eta})$ denotes the likelihood function, and $\chi(\boldsymbol{\eta})$ denotes the prior distribution of $\boldsymbol{\eta}$. Hence, the general FIM for the parameter vector, $\boldsymbol{\eta}$, is the sum of the FIM obtained from the likelihood due to the observations defined as $\mathbf{J}_{\boldsymbol{y}|\boldsymbol{\eta}}$ and the FIM from *a priori* information about the parameter vector defined as $\mathbf{J}_{\boldsymbol{\eta}}$.

Although the general FIM provides a way of quantifying the information about channel parameters present in random observations of the received signal, a more useful quantification metric could be the EFIM. The EFIM is more useful when the quantification of all the parameters in the parameter vector is not needed. Mathematically, given a parameter vector $\boldsymbol{\eta}$ that can be divided into a collection of useful parameters, $\boldsymbol{\eta}_1$, and nuisance parameters, $\boldsymbol{\eta}_2$, the general FIM has the following structure

$$\mathbf{J}_{\boldsymbol{y};\boldsymbol{\eta}} = \begin{bmatrix} \mathbf{J}_{\boldsymbol{y};\boldsymbol{\eta}_1} & \mathbf{J}_{\boldsymbol{y};\boldsymbol{\eta}_1,\boldsymbol{\eta}_2} \\ \mathbf{J}_{\boldsymbol{y};\boldsymbol{\eta}_1,\boldsymbol{\eta}_2}^{\mathrm{T}} & \mathbf{J}_{\boldsymbol{y};\boldsymbol{\eta}_2} \end{bmatrix},$$

where $\boldsymbol{\eta} \in \mathbb{R}^N, \boldsymbol{\eta}_1 \in \mathbb{R}^n, \mathbf{J}_{\boldsymbol{y};\boldsymbol{\eta}_1} \in \mathbb{R}^{n\times n}, \mathbf{J}_{\boldsymbol{y};\boldsymbol{\eta}_1,\boldsymbol{\eta}_2} \in \mathbb{R}^{n\times(N-n)}$, and $\mathbf{J}_{\boldsymbol{y};\boldsymbol{\eta}_2} \in \mathbb{R}^{(N-n)\times(N-n)}$ with $n < N$, and the EFIM [21] of parameter $\boldsymbol{\eta}_1$ is given by[1]

$$\mathbf{J}_{\boldsymbol{y};\boldsymbol{\eta}_1}^{\mathrm{e}} = \mathbf{J}_{\boldsymbol{y};\boldsymbol{\eta}_1} - \mathbf{J}_{\boldsymbol{y};\boldsymbol{\eta}_1}^{nu} = \mathbf{J}_{\boldsymbol{y};\boldsymbol{\eta}_1} - \mathbf{J}_{\boldsymbol{y};\boldsymbol{\eta}_1,\boldsymbol{\eta}_2}\mathbf{J}_{\boldsymbol{y};\boldsymbol{\eta}_2}^{-1}\mathbf{J}_{\boldsymbol{y};\boldsymbol{\eta}_1,\boldsymbol{\eta}_2}^{\mathrm{T}}.the \tag{20}$$

This EFIM captures all the required information about the parameters of interest present in the FIM; as observed from the relation $(\mathbf{J}_{\boldsymbol{y};\boldsymbol{\eta}_1}^{\mathrm{e}})^{-1} = [\mathbf{J}_{\boldsymbol{y};\boldsymbol{\eta}}^{-1}]_{[1:n,1:n]}$. To derive the entries in the FIM, we consider that the signal received in the DD domain is independent across N_U antennas and $N_n N_w$ DD resource elements. The resulting likelihood conditioned on the vector of channel parameters is $\chi(y_u[k,p]|\boldsymbol{\eta}) \propto \exp\left\{\frac{2}{N_0}\Re\left\{\mu_u^{\mathrm{H}}[k,p]y_u[k,p]\right\} - \frac{1}{N_0}\|\mu_u[k,p]\|_2^2\right\}$. The FIM due to observations, $\mathbf{J}_{\boldsymbol{y}|\boldsymbol{\eta}}$, is obtained by using the likelihood appropriately in (19). The resulting FIM has several submatrices, and each can be obtained using

$$\begin{aligned}&[\mathbf{J}_{\boldsymbol{y}|\boldsymbol{\eta}}]_{[v,g]} \\ &= \frac{2}{N_0}\sum_{u=1}^{N_U}\sum_{k=0}^{N_n-1}\sum_{p=0}^{N_w-1}\Re\left\{\nabla_{[\boldsymbol{\eta}]_{[v]}}^{\mathrm{H}}\mu_u[k,p]\nabla_{[\boldsymbol{\eta}]_{[g]}}\mu_u[k,p]\right\},\end{aligned} \tag{21}$$

where the derivatives, $\nabla_{[\boldsymbol{\eta}]_{[g]}}\mu_u[k,p]$, $g \in \boldsymbol{\eta}$ are presented in Section III-C.

Assuming that the paths are independent of each other, the FIM due to the *a priori* information about the channel parameters is $\mathbf{J}_{\boldsymbol{\eta}} = \mathrm{diag}\left[\mathbf{J}_{\boldsymbol{\eta}^{[0]}}, \mathbf{J}_{\boldsymbol{\eta}^{[1]}}, \cdots, \mathbf{J}_{\boldsymbol{\eta}^{[M_1]}}\right]$, where $\mathbf{J}_{\boldsymbol{\eta}^{[0]}}$ is the FIM due to the *a priori* information about the LOS related channel parameters and $\mathbf{J}_{\boldsymbol{\eta}^{[m]}}$ is the FIM due to the *a priori* information about the channel parameters related to the m^{th} RIS path. The resulting general FIM has dimensions of $7(M_1 \times 1)$ by $7(M_1 \times 1)$ and is obtained by summing the FIM obtained from the likelihood due to the observations defined as $\mathbf{J}_{\boldsymbol{y}|\boldsymbol{\eta}}$ and the FIM from *a priori* information about the parameter vector defined as $\mathbf{J}_{\boldsymbol{\eta}}$.

C. First Derivatives

The entries of the FIM due to the observations are complicated, and closed-form expressions are not presented. Instead, the first derivatives of the expressions of the received signals are presented. To present these derivatives, we first present derivatives of the expression of the channel in the DD domain. The derivatives of the expression of the channel in the DD domain with respect to $\boldsymbol{\eta}_a^{[0]} = \boldsymbol{\eta}^{[0]}/\nu_{B,U}^{[0]}$ and $\nu_{B,U}^{[0]}$ are presented in (24) and (25), respectively. The RIS paths are similar, hence we focus on the m^{th} RIS-path, the derivatives with respect to $\boldsymbol{\eta}_a^{[m]} = \boldsymbol{\eta}^{[m]}/[\nu_{R,U}^{[m]}, \boldsymbol{\Phi}_R^{[m]}]$, $\nu_{R,U}^{[m]}$, and $\boldsymbol{\Phi}_R^{[m]}$ are presented in (26), (27), and (28) respectively. The derivatives with respect to the useful parameters $\nabla_{[\boldsymbol{\eta}_a^{[0]}]_{[v]}}\tau_{b,u}^{[0]}$, $\nabla_{[\boldsymbol{\eta}_a^{[m]}]_{[v]}}\tau_{r,u}^{[m]}$, $\nabla_{[\boldsymbol{\Phi}_R^{[m]}]}\tau_{b,r}^{[m]}$, and $\nabla_{[\boldsymbol{\Phi}_R^{[m]}]}\tau_{r,u}^{[m]}$ are easy to derive and can be found in the appendix of [5].

[1]This is also applicable to the FIM due to observations, $\mathbf{J}_{\boldsymbol{y}|\boldsymbol{\eta}_1}^{\mathrm{e}} = \mathbf{J}_{\boldsymbol{y}|\boldsymbol{\eta}_1} - \mathbf{J}_{\boldsymbol{y}|\boldsymbol{\eta}_1}^{nu}$.

$$H_{b,u}[k^{'},p^{'}]=N_w\beta_{b,u}^{[0]}e^{j2\pi\nu_{b,u}^{[0]}\frac{p^{'}}{\Delta f N_w}}\sum_n e^{-\frac{j2\pi}{N_n}(k-k^{'}-\nu_{b,u}^{[0]}N_nT)n}\sum_w e^{-\frac{j2\pi}{N_w}(p^{'}+\tau_{b,u}^{[0]}N_w\Delta f-p)w}\begin{cases}1 & \text{if } a=1\\ e^{-j2\pi\left(\frac{k'}{N_n}+\nu_{b,u}^{[0]}T\right)} & \text{if } a=2\end{cases}, \tag{22}$$

$$H_{b,u}^{r,[m]}[k^{'},p^{'}]=N_w\beta_{b,r}^{[m]}\beta_{r,u}^{[m]}e^{j2\pi\nu_{r,u}^{[m]}\tau_{b,r}^{[m]}}e^{j2\pi(\nu_{b,r}^{[m]}+\nu_{r,u}^{[m]})T\frac{p^{'}}{N_w}}\sum_n e^{-\frac{j2\pi}{N_n}2\pi(k-k^{'}-(\nu_{b,r}^{[m]}+\nu_{r,u}^{[m]})N_nT)n}\times$$
$$\sum_w e^{\frac{j2\pi}{N_w}2\pi(p^{'}-p-(\tau_{b,r}^{[m]}+\tau_{r,u}^{[m]})N_w\Delta f)w}\begin{cases}1 & \text{if } a=1\\ e^{-j2\pi\left(\frac{k'}{N_n}+(\nu_{b,r}^{[m]}+\nu_{r,u}^{[m]})T\right)} & \text{if } a=2\end{cases}, \tag{23}$$

$$\nabla_{[\boldsymbol{\eta}_a^{[0]}]_{[v]}}H_{b,u}[k^{'},p^{'}]=(-j2\pi\nabla_{[\boldsymbol{\eta}_a^{[0]}]_{[v]}}\tau_{b,u}^{[0]})N_w\sum_{n,w}\beta_{b,u}^{[0]}e^{j2\pi\nu_{b,u}^{[0]}\frac{p^{'}}{\Delta f N_w}}e^{-\frac{j2\pi}{N_n}(k-k^{'}-\nu_{b,u}^{[0]}N_nT)n}e^{-\frac{j2\pi}{N_w}(p^{'}+\tau_{b,u}^{[0]}N_w\Delta f-p)w}\times$$
$$\begin{cases}w\Delta f & \text{if } a=1\\ w\Delta f e^{-j2\pi\left(\frac{k'}{N_n}+\nu_{b,u}^{[0]}T\right)} & \text{if } a=2\end{cases}. \tag{24}$$

$$\nabla_{\nu_{B,U}^{[0]}}H_{b,u}[k^{'},p^{'}]=j2\pi N_w\sum_{n,w}\beta_{b,u}^{[0]}e^{j2\pi\nu_{b,u}^{[0]}\frac{p^{'}}{\Delta f N_w}}e^{-\frac{j2\pi}{N_w}(p^{'}+\tau_{b,u}^{[0]}N_w\Delta f-p)w}\times$$
$$\begin{cases}\frac{p^{'}}{\Delta f N_w}\nabla_{\nu_{B,U}^{[0]}}\nu_{b,u}^{[0]}\sum_n e^{-\frac{j2\pi}{N_n}(k-k^{'}-\nu_{b,u}^{[0]}N_nT)n}+\nabla_{\nu_{B,U}^{[0]}}\nu_{b,u}^{[0]}\sum_n nTe^{-\frac{j2\pi}{N_n}(k-k^{'}-\nu_{b,u}^{[0]}N_nT)n} & \text{if } a=1\\ (\frac{p^{'}}{\Delta f N_w}-T)\nabla_{\nu_{B,U}^{[0]}}\nu_{b,u}^{[0]}\sum_n e^{-\frac{j2\pi}{N_n}(k-k^{'}-\nu_{b,u}^{[0]}N_nT)n}+\nabla_{\nu_{B,U}^{[0]}}\nu_{b,u}^{[0]}\sum_n nTe^{-\frac{j2\pi}{N_n}(k-k^{'}-\nu_{b,u}^{[0]}N_nT)n} & \text{if } a=2\end{cases}. \tag{25}$$

$$\nabla_{[\boldsymbol{\eta}_a^{[m]}]_{[v]}}H_{b,u}^{r,[m]}[k^{'},p^{'}]=-j2\pi N_w\beta_{b,r}^{[m]}\beta_{r,u}^{[m]}e^{j2\pi\nu_{r,u}^{[m]}\tau_{b,r}^{[m]}}e^{j2\pi(\nu_{b,r}^{[m]}+\nu_{r,u}^{[m]})T\frac{p^{'}}{N_w}}\sum_n e^{-\frac{j2\pi}{N_n}2\pi(k-k^{'}-(\nu_{b,r}^{[m]}+\nu_{r,u}^{[m]})N_nT)n}\times$$
$$\sum_w we^{\frac{j2\pi}{N_w}2\pi(p^{'}-p-(\tau_{b,r}^{[m]}+\tau_{r,u}^{[m]})N_w\Delta f)w}\begin{cases}(\nabla_{[\boldsymbol{\eta}_a^{[m]}]_{[v]}}\tau_{r,u}^{[m]}\Delta f) & \text{if } a=1\\ (\nabla_{[\boldsymbol{\eta}_a^{[m]}]_{[v]}}\tau_{r,u}^{[m]}\Delta f)e^{-j2\pi\left(\frac{k'}{N_n}+(\nu_{b,r}^{[m]}+\nu_{r,u}^{[m]})T\right)} & \text{if } a=2\end{cases}, \tag{26}$$

$$\nabla_{\nu_{R,U}^{[m]}}H_{b,u}^{r,[m]}[k^{'},p^{'}]=j2\pi N_w\beta_{b,r}^{[m]}\beta_{r,u}^{[m]}e^{j2\pi\nu_{r,u}^{[m]}\tau_{b,r}^{[m]}}e^{j2\pi(\nu_{b,r}^{[m]}+\nu_{r,u}^{[m]})T\frac{p^{'}}{N_w}}\sum_w e^{\frac{j2\pi}{N_w}2\pi(p^{'}-p-(\tau_{b,r}^{[m]}+\tau_{r,u}^{[m]})N_w\Delta f)w}\times$$
$$\begin{cases}\nabla_{\nu_{R,U}^{[m]}}\nu_{r,u}^{[m]}\left[(\frac{p^{'}}{\Delta f N_w}+\tau_{b,r}^{[m]})\sum_n e^{-\frac{j2\pi}{N_n}(k-k^{'}-(\nu_{b,r}^{[m]}+\nu_{r,u}^{[m]})N_nT)n}+\sum_n nTe^{-\frac{j2\pi}{N_n}(k-k^{'}-(\nu_{b,r}^{[m]}+\nu_{r,u}^{[m]})N_nT)n}\right] & \text{if } a=1\\ \nabla_{\nu_{R,U}^{[m]}}\nu_{r,u}^{[m]}\left[(\frac{p^{'}}{\Delta f N_w}+\tau_{b,r}^{[m]}-T)\sum_n e^{-\frac{j2\pi}{N_n}(k-k^{'}-(\nu_{b,r}^{[m]}+\nu_{r,u}^{[m]})N_nT)n}+\sum_n nTe^{-\frac{j2\pi}{N_n}(k-k^{'}-(\nu_{b,r}^{[m]}+\nu_{r,u}^{[m]})N_nT)n}\right] & \text{if } a=2\end{cases}, \tag{27}$$

$$\nabla_{\boldsymbol{\Phi}^{[m]}}H_{b,u}^{r,[m]}[k^{'},p^{'}]=j2\pi N_w\beta_{b,r}^{[m]}\beta_{r,u}^{[m]}e^{j2\pi\nu_{r,u}^{[m]}\tau_{b,r}^{[m]}}e^{j2\pi(\nu_{b,r}^{[m]}+\nu_{r,u}^{[m]})T\frac{p^{'}}{N_w}}\sum_n e^{-\frac{j2\pi}{N_n}2\pi(k-k^{'}-(\nu_{b,r}^{[m]}+\nu_{r,u}^{[m]})N_nT)n}\times$$
$$\sum_w e^{\frac{j2\pi}{N_w}2\pi(p^{'}-p-(\tau_{b,r}^{[m]}+\tau_{r,u}^{[m]})N_w\Delta f)w}\begin{cases}(\nu_{r,u}^{[m]}\nabla_{\boldsymbol{\Phi}^{[m]}}(\tau_{b,r}^{[m]})-\nabla_{\boldsymbol{\Phi}^{[m]}}(\tau_{b,r}^{[m]}+\tau_{r,u}^{[m]})w\Delta f) & \text{if } a=1\\ (\nu_{r,u}^{[m]}\nabla_{\boldsymbol{\Phi}^{[m]}}(\tau_{b,r}^{[m]})-\nabla_{\boldsymbol{\Phi}^{[m]}}(\tau_{b,r}^{[m]}+\tau_{r,u}^{[m]})w\Delta f)e^{-j2\pi\left(\frac{k'}{N_n}+(\nu_{b,r}^{[m]}+\nu_{r,u}^{[m]})T\right)} & \text{if } a=2\end{cases}. \tag{28}$$

It is reasonable to assume that $\nu_{B,U}^{[0]}=\nu_{b,u}^{[0]},\forall b,\forall u$. Hence, $\nabla_{\nu_{B,U}^{[0]}}\nu_{b,u}^{[0]}=1,\forall b,\forall u$. Also, it is reasonable to assume that for the m^{th} RIS path, $\nu_{R,U}^{[m]}=\nu_{r,u}^{[m]},\forall r,\forall u$. Hence, $\nabla_{\nu_{R,U}^{[m]}}\nu_{r,u}^{[m]}=1,\forall r,\forall u$. With the derivatives of

the expressions of the channel, the first derivatives of the expressions of the received signals can be presented.

Lemma 6. *The first derivatives of the expressions for the LOS part of the received signals is described as*

$$\nabla_{\boldsymbol{\eta}^{[0]}}\mu_u^{(1,a)}[k,p] = \frac{1}{N_n N_w^2} \times \left[\sum_b \sum_{k'} \sum_{p'} \mathsf{x}_b[k',p']\nabla_{\boldsymbol{\eta}^{[0]}} H_{b,u}[k',p']\right], \tag{29}$$

where $a \in \{1,2\}$, and the channel is given by (22). If $a = 1$ then $p' \in [0, N_w - 1 - p_{l,b,u}]$, $a = 2$ then $p' \in [N_w - p_{l,b,u}, N_w - 1]$.

Proof. The proof is straightforward, as derivatvies are distributive and the transmit signal, $\mathsf{x}_b[k',p']$, does not depend on the parameter vector, $\boldsymbol{\eta}^{[0]}$. □

Lemma 7. *The first derivatives of the expressions of the part of the received signal that is reflected by the RISs and received at the u^{th} antenna is described as*

$$\nabla_{\boldsymbol{\eta}^{[m]}}\mu_u^{(2,a)}[k,p] = \frac{1}{N_w^2 N_n}\sum_{m=1}^{M_1}\psi^{[m]}\sum_b\sum_{r=1}^{N_R^{[m]}} \times e^{j\vartheta_r^{[m]}}\sum_{k'}\sum_{p'}\mathsf{x}_b[k',p']\nabla_{\boldsymbol{\eta}^{[m]}}\left[H_{b,u}^{r,[m]}[k',p']\right], \tag{30}$$

where $a \in \{1,2\}$, and the channel is (23). If $a = 1$ then $p' \in [0, N_w - (p_{l_1,b,r}^{[m]} + p_{l_2,r,u}^{[m]}) - 1]$, $a = 2$ then $p' \in [N_w - (p_{l_1,b,r}^{[m]} + p_{l_2,r,u}^{[m]}), N_w - 1]$.

Proof. The proof is straightforward, as derivatvies are distributive and the transmit signal, $\mathsf{x}_b[k',p']$, does not depend on the parameter vector, $\boldsymbol{\eta}^{[m]}$. □

Corollary 5. *The first derivatives of the expression representing the signal in the DD domain from both the LOS path and the RISs, which is received at the u^{th} antenna, and needed in (21), is*

$$\nabla_{\boldsymbol{\eta}}\mu_u[k,p] = \nabla_{\boldsymbol{\eta}}\mu_u^{(1)}[k,p] + \nabla_{\boldsymbol{\eta}}\mu_u^{(2)}[k,p]. \tag{31}$$

Proof. The proof is straightforward, as derivatvies are distributive. □

The FIM due to observations, $\mathbf{J}_{\boldsymbol{y}|\boldsymbol{\eta}}$, can be constructed by substituting (21) in Corollary 5. Subsequently, the general FIM, $\mathbf{J}_{\boldsymbol{\eta};\boldsymbol{\eta}}$ can be obtained by substituting the FIM due to observations, $\mathbf{J}_{\boldsymbol{y}|\boldsymbol{\eta}}$, and the FIM due to *a priori* information, $\mathbf{J}_{\boldsymbol{\eta}}$, into (19).

D. Fisher Information Matrix for Location Parameters

The available information about the UE location parameters and the RIS orientation offset can be jointly calculated by transforming the FIM of the channel parameters. To achieve this transformation, we define the location parameters. The UE location parameter is defined as $\boldsymbol{\kappa}_0 = \left[\boldsymbol{p}_U^{\mathrm{T}}, \boldsymbol{\Phi}_U^{\mathrm{T}}\right]^{\mathrm{T}}$. With this, the location parameters (UE location and RISs' orientation offset) are represented as $\boldsymbol{\kappa} \triangleq \left[\boldsymbol{\kappa}_0^{\mathrm{T}}, \boldsymbol{\Phi}^{[1]\mathrm{T}}, \cdots, \boldsymbol{\Phi}^{[M_1]\mathrm{T}}\right]^{\mathrm{T}}$. Now, the transformation of the FIM of the channel parameters to the FIM of the location parameters is obtained using $\mathbf{J}_{\boldsymbol{y}|\boldsymbol{\kappa}} \triangleq \boldsymbol{\Upsilon}_{\boldsymbol{\kappa}}\mathbf{J}_{\boldsymbol{y}|\boldsymbol{\eta}_1}^{\mathrm{e}}\boldsymbol{\Upsilon}_{\boldsymbol{\kappa}}^{\mathrm{T}}$, where $\boldsymbol{\Upsilon}_{\boldsymbol{k}}$ represents derivatives of the non-linear relationship between the channel parameters and the location parameters. The entries in the matrix $\boldsymbol{\Upsilon}_{\boldsymbol{\kappa}}$ are presented in Appendix E of [5]. The general FIM, $\mathbf{J}_{\boldsymbol{y};\boldsymbol{\kappa}}$, of the location parameters can be obtained using (19) and it is $\mathbf{J}_{\boldsymbol{y};\boldsymbol{\kappa}} = \mathbf{J}_{\boldsymbol{y}|\boldsymbol{\kappa}} + \mathbf{J}_{\boldsymbol{\kappa}}$, where $\mathbf{J}_{\boldsymbol{\kappa}}$ is a diagonal matrix representing the *a priori* information about the location parameters.

E. Position and Orientation Error Bounds

The position and orientation error of the UE can be calculated by inverting $\mathbf{J}_{\boldsymbol{y};\boldsymbol{\kappa}}$ and summing the appropriate diagonals. The position error bound (PEB) of the UE is found by summing the first three diagonals of $\mathbf{J}_{\boldsymbol{y};\boldsymbol{\kappa}}^{-1}$, the orientation error bound (OEB) of the UE is found by summing the next three diagonals of $\mathbf{J}_{\boldsymbol{y};\boldsymbol{\kappa}}^{-1}$. Similarly, the orientation error bound (OEB$^{[m]}$) of the m^{th} RIS can be obtained by summing the appropriate diagonals of $\mathbf{J}_{\boldsymbol{y};\boldsymbol{\kappa}}^{-1}$.

IV. Numerical Results

In this section, we use simulations to characterize the PEB of the UE. We also present the OEB$^{[1]}$ of the first RIS. The system setup consists of a blocked LOS path with $M_1 = 2$ RISs providing reflections from a single antenna BS (located at $\boldsymbol{p}_B = [0,0,0]^{\mathrm{T}}$ with $\boldsymbol{Q}_B = \boldsymbol{I}$) to a UE (located at $\boldsymbol{p}_U = [10, 8.2, 4]^{\mathrm{T}}$ with $\boldsymbol{Q}_U = \boldsymbol{I}$). We assume that there are 25 DDRE, with $N_n = 5$, and $N_w = 5$. The Doppler is set to 10 for all paths and $\Delta f = 15$ kHz. We consider free space pathloss, with transmit and receive antenna gains of 2 dB, no transmit beamforming, a transmit power of 23 dBm, and the noise power spectral density (PSD) is $N_0 = -174$ dBm/Hz. The first RIS has its centroid located at $\boldsymbol{p}_R^{[1]} = [10, 8, 4]^{\mathrm{T}}$ with the following rotation angles $\boldsymbol{\Phi}_R^{[1]} = [0.1, 0.2, 0.1]^{\mathrm{T}}$, while the second RIS is located at $\boldsymbol{p}_R^{[2]} = [10, 8.5, 4]^{\mathrm{T}}$ with $\boldsymbol{Q}_R^{[2]} = \boldsymbol{I}$. The orientation of the first RIS is unknown, and the orientation of the second RIS is known. We assume uniform rectangular arrays (URA) at all communication entities. With the considered user position and the Fraunhofer distance [17], the UE is in the near-field of the first RIS when $N_R^{[1]} \geq 64$ and in the near-field of the second RIS when $N_R^{[2]} \geq 64$.

A. PEB of the UE

We present the PEB of the UE when it experiences near-field propagation in relation to both RISs under three cases. In all three cases, no *a priori* information is available, and a varying number of receive antennas and RIS elements are considered. In Case (a), the UE only uses the reflected signal from the misoriented RIS to find its position. In this

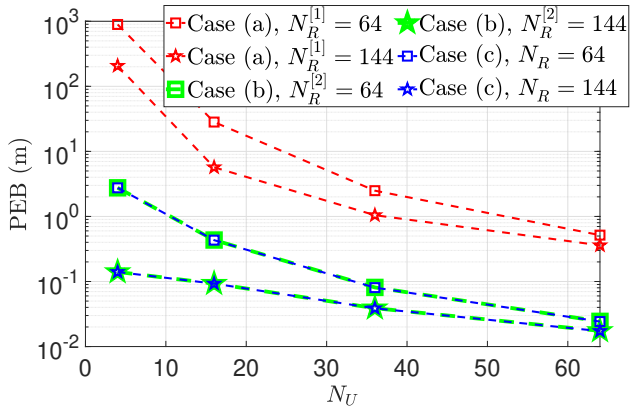

Figure 2. PEB of UE vs. N_U.

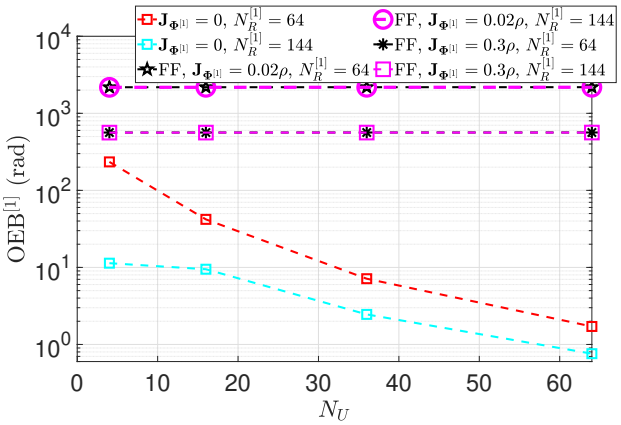

Figure 3. OEB$^{[1]}$ vs. N_U.

case, the RIS orientation offset and the complex path gains are nuisance parameters. Hence, this case demonstrates the impact of the RIS orientation offset on the PEB of the UE. In Case (b), the UE only uses the reflected signals from the second RIS (whose orientation is known) to find its position. In this case, the complex path gains are nuisance parameters.

Finally, in Case (c), reflected signals from both RISs are used to position the UE. From Fig. 2, in all cases, the PEB decreases with an increase in the number of receive antennas and RIS elements.

B. OEB of the First RIS

We present OEB$^{[1]}$ when the UE utilizes the received signal at the UE while it experiences near-field propagation effects in relation to the first RIS to quantify the available information about the orientation offset of the first RIS. We consider two cases. In the first case, the UE assumes *correctly* that it is experiencing near-field propagation and uses the appropriate equations to quantify the available information about $\mathbf{\Phi}^{[1]}$. In the second case, the UE assumes *incorrectly* that it is experiencing far-field propagation and attempts to use inappropriate equations to quantify the available information about $\mathbf{\Phi}^{[1]}$.

In all applicable plots, the prefix "FF" is used to distinguish the *incorrect* case where a far-field model is applied to this near-field simulation setup from the *correct* case where the near-field model is used for the near-field setup. In both cases, the only *a priori* information available is about the orientation offset. Hence, $\mathbf{J}_{\boldsymbol{\kappa}}$ is a zero matrix, except at the diagonal entry corresponding to $\mathbf{\Phi}^{[1]}$. This entry, $\mathbf{J}_{\mathbf{\Phi}^{[1]}}$, and the information it conveys is quantified as a fraction of the SNR, ρ.

From Fig 3, when the near-field model is *correctly* used, the OEB decreases with an increase in N_U and $N_R^{[1]}$. However, the OEB for a specific $N_R^{[1]}$ and *a priori* information remains constant for varying N_U when the far-field model is *incorrectly* used. Hence, we can conclude that the number of receive antennas only affects the estimation accuracy of the RIS orientation offset when the UE is in the near-field of the RIS.

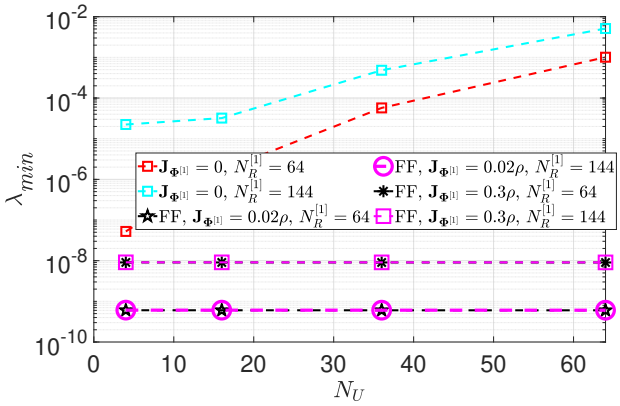

Figure 4. The smallest eigenvalue, λ_{min}, of $\mathbf{J}_{\boldsymbol{y};\boldsymbol{\kappa}}$ vs. N_U.

The constant OEB$^{[1]}$ when the far-field model is *incorrectly* used can be explained by observing that the smallest eigenvalue of $\mathbf{J}_{\boldsymbol{y};\boldsymbol{\kappa}}$, λ_{min} remains constant for increasing N_U [2]. In Fig. 4, while using the near-field model, the smallest eigenvalue increases significantly with an increase in N_U, when using the far-field model, the smallest eigenvalue stays relatively constant irrespective of N_U. This observation implies that in the far-field, the OEB is independent of N_U and only depends on the *a priori* information.

V. Conclusion

This paper has investigated the fundamental limits of RIS-aided OTFS systems for localization. To obtain these limits, we derived the received signal expressions in the

[2]The smallest eigenvalue is significant because $\mathbf{J}_{\boldsymbol{y};\boldsymbol{\kappa}}$ is at least positive definite. Hence, a small eigenvalue close to zero implies that the matrix is almost non-invertible. This, in turn, leads to high OEB.

DD when the system experiences the effects of near-field or far-field propagation. Subsequently, these received signal expressions and the FIM are used to provide the fundamental limits for localization. Through simulations, we showed that the localization error decreases with the number of receive antennas and RIS elements. Furthermore, considering that the orientation of the RISs can be disturbed after initial deployment, we also investigated the possibility of using the signals received at the UE in the DD domain to estimate the RIS orientation. Our results indicate that the orientation of a certain RIS can only be estimated when the UE experiences the effects of near-field propagation with respect to that RIS. We also showed that a fundamental drawback of RIS-aided localization of a UE is that the RIS orientation offset is detrimental to the localization error of the UE.

REFERENCES

[1] Z. Abu-Shaban, G. Seco-Granados, C. R. Benson, and H. Wymeersch, "Performance analysis for autonomous vehicle 5g-assisted positioning in GNSS-challenged environments," in *2020 IEEE/ION PLANS*, 2020, pp. 996–1003.

[2] T. Gerratt, A. Strate, and R. Christensen, "Navigation error sensitivity of autonomous carrier landing systems in GPS-denied environments," in *2020 IEEE/ION PLANS*, 2020, pp. 81–90.

[3] D.-R. Emenonye, H. S. Dhillon, and R. M. Buehrer, "Fundamentals of RIS-aided localization in the far-field," *submitted to* IEEE Trans. on Wireless Commun.*, available online: arxiv.org/abs/2206.01652*, 2022.

[4] ——, "Estimation of RIS misorientation in both near and far field regimes," *accepted to Proc., IEEE Intl. Conf. on Commun. (ICC)*, 2023.

[5] ——, "RIS-aided localization under position and orientation offsets in the near and far field," submitted to *IEEE Trans. on Wireless Commun., available online: arxiv.org/abs/2210.03599*, 2022.

[6] A. Elzanaty, A. Guerra, F. Guidi, and M.-S. Alouini, "Reconfigurable intelligent surfaces for localization: Position and orientation error bounds," *IEEE Trans. on Signal Processing*, vol. 69, pp. 5386–5402, Aug. 2021.

[7] R. Hadani, S. Rakib, M. Tsatsanis, A. Monk, A. J. Goldsmith, A. F. Molisch, and R. Calderbank, in *Proc., IEEE Wireless Commun. and Networking Conf. (WCNC)*.

[8] P. Raviteja, K. T. Phan, Y. Hong, and E. Viterbo, "Interference cancellation and iterative detection for orthogonal time frequency space modulation," *IEEE Trans. on Wireless Commun.*, vol. 17, no. 10, pp. 6501–6515, Oct 2018.

[9] W. Shen, L. Dai, J. An, P. Fan, and R. W. Heath, "Channel estimation for orthogonal time frequency space (OTFS) massive MIMO," *IEEE Trans. on Signal Processing*, vol. 67, no. 16, pp. 4204–4217, Apr. 2019.

[10] M. Z. Win, Z. Wang, Z. Liu, Y. Shen, and A. Conti, "Location awareness via intelligent surfaces: A path toward holographic NLN," *IEEE Veh. Technology Magazine*, vol. 17, no. 2, pp. 37–45, June 2022.

[11] Z. Wang, Z. Liu, Y. Shen, A. Conti, and M. Z. Win, "Location awareness in beyond 5G networks via reconfigurable intelligent surfaces," *IEEE J. Sel. Areas Commun.*, vol. 40, no. 7, pp. 2011–2025, July 2022.

[12] S. Hu, F. Rusek, and O. Edfors, "Beyond massive MIMO: The potential of positioning with large intelligent surfaces," *IEEE Trans. on Signal Processing*, vol. 66, no. 7, pp. 1761–1774, Apr. 2018.

[13] Z. Abu-Shaban, K. Keykhosravi, M. F. Keskin, G. C. Alexandropoulos, G. Seco-Granados, and H. Wymeersch, "Near-field localization with a reconfigurable intelligent surface acting as lens," in *Proc., IEEE Intl. Conf. on Commun. (ICC)*, 2021.

[14] A. Fascista, M. F. Keskin, A. Coluccia, H. Wymeersch, and G. Seco-Granados, "RIS-aided joint localization and synchronization with a single-antenna receiver: Beamforming design and low-complexity estimation," *IEEE J. of Sel. Topics in Signal Processing*, to appear.

[15] K. Keykhosravi, M. F. Keskin, S. Dwivedi, G. Seco-Granados, and H. Wymeersch, "Semi-passive 3D positioning of multiple RIS-enabled users," *IEEE Trans. on Veh. Technology*, vol. 70, no. 10, pp. 11 073–11 077, Oct. 2021.

[16] K. Keykhosravi, M. F. Keskin, G. Seco-Granados, P. Popovski, and H. Wymeersch, "RIS-enabled SISO localization under user mobility and spatial-wideband effects," *IEEE J. of Sel. Topics in Signal Processing*, pp. 1–1, to appear.

[17] F. Guidi and D. Dardari, "Radio positioning with EM processing of the spherical wavefront," *IEEE Trans. on Wireless Commun.*, vol. 20, no. 6, pp. 3571–3586, Jan. 2021.

[18] C. Xu, L. Xiang, J. An, C. Dong, S. Sugiura, R. G. Maunder, L.-L. Yang, and L. Hanzo, "OTFS-aided RIS-assisted SAGIN systems outperform their OFDM counterparts in doubly selective high-Doppler scenarios," *IEEE Internet Things J.*, vol. 10, no. 1, pp. 682–703, Jan, 2023.

[19] V. S. Bhat, G. Harshavardhan, and A. Chockalingam, "Input-output relation and performance of RIS-aided OTFS with fractional delay-Doppler," *IEEE Communications Letters*, vol. 27, no. 1, pp. 337–341, Jan, 2023.

[20] S. M. LaValle, *Planning Algorithms*. Cambridge University Press, 2006.

[21] Y. Shen and M. Z. Win, "Fundamental limits of wideband localization — part I: A general framework," *IEEE Trans. on Info. Theory*, vol. 56, no. 10, pp. 4956–4980, Oct. 2010.